IEEE Photonics Journal
An IEEE Photonics Society Publication

Open Access

Dual Metamaterial With Large Birefringence

Volume 7, Number 6, December 2015

Li Min
Li-Rong Huang
Rong Sun
Man-Man Xi
Zhi-Wei Li

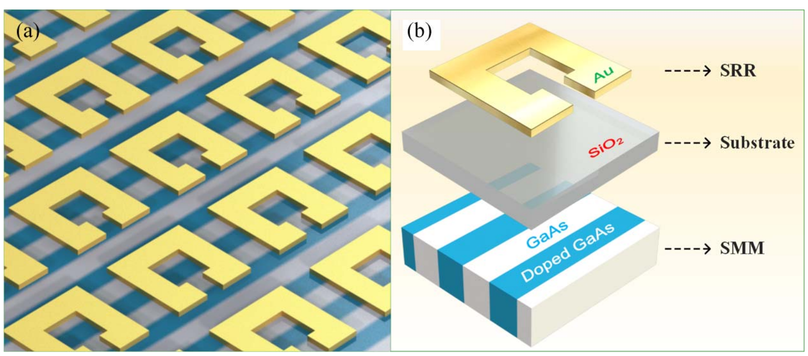

DOI: 10.1109/JPHOT.2015.2497228
1943-0655 © 2015 IEEE

Dual Metamaterial With Large Birefringence

Li Min, Li-Rong Huang, Rong Sun, Man-Man Xi, and Zhi-Wei Li

Wuhan National Laboratory for Optoelectronics, School of Optical and Electronic Information, Huazhong University of Science and Technology, Wuhan 430074, China

DOI: 10.1109/JPHOT.2015.2497228

Manuscript received June 1, 2015; revised October 28, 2015; accepted October 29, 2015. Date of publication November 2, 2015; date of current version November 10, 2015. This work was supported in part by the Specialized Research Fund for the Doctoral Program of Higher Education (SRFDP) under Grant 20120142110064 and in part by the National Natural Science Foundation of China under Grant 11104093 and Grant 11474116. Corresponding author: L.-R. Huang (e-mail: lrhuang@hust.edu.cn).

Abstract: Strong birefringence and a large phase delay are highly desirable for high-efficiency and compact wave plates. In order to enhance the phase delay, we combine a semiconductor metamaterial (SMM) and split-ring resonators (SRRs) into a novel dual metamaterial, which exhibits two types of resonance response, i.e., one type is mainly induced by the SMM for one polarization component of the incident wave, and the other is mainly induced by the SRRs for the other orthogonal polarization component. The unique resonance characteristics lead to large birefringence and, hence, a considerable phase delay, enabling the realization of a very compact quarter-wave plate in the middle-infrared spectrum. The concept of the dual metamaterial has the potential for developing ultracompact high-performance microoptical/nanooptical components.

Index Terms: Metamaterials, resonance, birefringence, split-ring resonators, semiconductor metamaterials.

1. Introduction

The control of optical phase has greatly affected our daily life, from consumer products to high-tech applications. Conventional wave plates use birefringence or total internal reflection effect of crystals and polymers [1]–[4]. In comparison with conventional wave plates, metamaterial wave plates usually have smaller volumes and are more suitable for compact optical components [5]–[10].

As we know, a wave plate is usually made of optical anisotropic materials, and the phase delay (or phase difference) $\Delta\varphi$ between the two orthogonally polarized components of an electromagnetic (EM) wave is given by [11]

$$\Delta\varphi = \frac{\omega d}{c}(n_\perp - n_{||}) \tag{1}$$

where ω denotes the frequency of an incident wave, c is the vacuum light velocity, d is the thickness of the wave plate, and $n_{||}$ and $n_\perp$ are the material refractive indices for the two orthogonally polarized components. Equation (1) tells us that, for a given thickness d, the phase delay $\Delta\varphi$ is dependent on the birefringence Δn ($\Delta n = n_\perp - n_{||}$), and a larger birefringence Δn results in a higher phase delay. Due to the unique resonance effects [7], [12]–[17], metamaterials usually have stronger birefringence Δn and, thus, can be used to construct much more compact wave plates than conventional materials, such as crystals, polymers, etc. For example, the

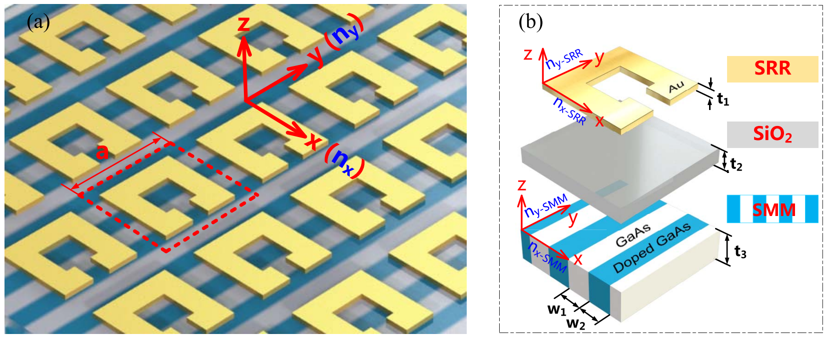

Fig. 1. (a) Schematic of a dual-metamaterial composed of a SMM and SRRs. (b) Unit structure of the dual-metamaterial.

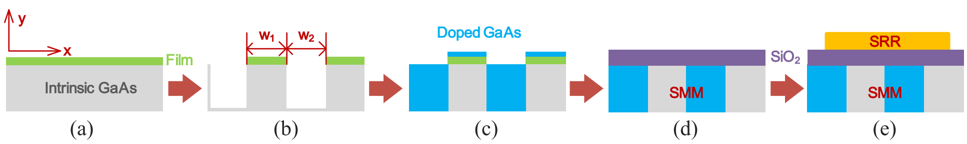

Fig. 2. Fabrication procedures of the dual-metamaterial. (a) Coat a mask film on the intrinsic GaAs layer. (b) Etch the intrinsic GaAs. (c) Grow the doped GaAs. (d) Remove the mask film, and deposit SiO_2. (e) Fabricate the Au SRRs.

thicknesses of conventional quarter-wave plates are usually larger than 450 μm [18]–[22], whereas metamaterial-based quarter-wave plates are usually smaller than 50 μm [6], [8], [21].

Considering the relationship among phase delay $(\Delta\varphi)$, birefringence (i.e., Δn), and thickness (d), it is natural for one to think that, if both $|n_{||}|$ and $|n_{\perp}|$ are designed to have higher values with opposite signs, or one of them is very large while the other is very low, then a bigger optical phase delay can be obtained, and this will be helpful for reducing the thickness and volume of the wave plate. In this paper, we construct a novel dual-metamaterial composed of a semiconductor metamaterial (SMM), a SiO_2 spacer layer and split ring resonators (SRRs), which can work as a very compact quarter-wave plate due to the EM resonances of the SMM and the SRRs.

2. Method

In order to achieve higher birefringence, one should make a metamaterial wave plate exhibiting strong resonance in the two orthogonal directions. As we know, both semiconductor metamaterials (SMMs) and split ring resonators (SRRs) are highly anisotropic, EM resonance effect can make them experience a large variation of the refractive index in one polarization direction, while not in the orthogonal polarization direction. In present work, we combine a SMM, a SiO_2 spacer layer and SRRs into a dual-metamaterial, as shown in Fig. 1(a). The dashed box in Fig. 1(a) represents a unit of the dual-metamaterial, and its layered structure is schematically depicted in Fig. 1(b). The lattice constant of the dual-metamaterial is $a = 2.5$ μm. For the gold SRR unit, its out-side length, inner-side length and split-width are 1.6 μm, 1.0 μm, and 0.1 μm, respectively; and its thickness t_1 is 0.08 μm, and for the SiO_2 layer, its thickness t_2 is 0.1 μm. The SMM is composed of intrinsic GaAs and doped GaAs materials, their thicknesses are both $t_3 = 0.4$ μm, and their widths are w_1 and w_2 $(w_1 = w_2 = 25$ nm), respectively.

We expect that, for the dual-metamaterial, the variation of the refractive index (i.e., n_x) in the x direction will be determined mainly by the SMM, while the variation of the refractive index (i.e., n_y) in the y direction will originate mainly from the SRRs. Before confirming these, we need to discuss the fabrication process of the dual-metamaterial. First, we should fabricate a SMM. A mask film is coated on an intrinsic GaAs layer as shown in Fig. 2(a); then, grooves with width w_2 and thickness t_3 are obtained by electronic-beam lithography and etching processes, as shown in Fig. 2(b). Then, an epitaxial growth is made for the doped GaAs, as seen in Fig. 2(c). After removing the mask film and the doped GaAs on it, a SMM, comprising interleaved intrinsic GaAs of width w_1 and doped GaAs of width w_2, is obtained. Next, a silicon dioxide (SiO_2) film is deposited on the SMM, as shown in Fig. 2(d). Finally, the dual-metamaterial can be obtained after the Au SRRs is fabricated by electronic-beam lithography, electronic beam evaporation and lift-off processes, as shown in Fig. 2(e).

3. Results and Discussions

In the following, we study the resonance properties of the dual-metamaterial by firstly investigating the effective permittivities of the SMM consisting of intrinsic GaAs (non-plasmonic material) and doped GaAs (plasmonic material). As we know, in the limit of subwavelength layer thickness, the effective permittivity of a multi-layered structure made from non-plasmonic and plasmonic materials can exhibit EM resonance at the designed wavelength, and this has been demonstrated with simulated and experimental results [23]. As refs [22]–[28] discussed, the effective permittivities ($\varepsilon_{x-\mathrm{SMM}}$ and $\varepsilon_{y-\mathrm{SMM}}$) of the proposed SMM in the x direction and the y direction can be calculated with quasi-static effective medium theory (EMT)

$$\varepsilon_{x-\mathrm{SMM}}^{-1} = (1-f)\varepsilon_i^{-1} + f\varepsilon_d^{-1} \tag{2}$$

$$\varepsilon_{y-\mathrm{SMM}} = (1-f)\varepsilon_i + f\varepsilon_d \tag{3}$$

where ε_i and ε_d are the permittivities of GaAs and doped GaAs, respectively; f is the filling fraction of the doped GaAs; and $f = w_2/(w_1 + w_2)$. The effective refractive indices of the SMM $n_{x-\mathrm{SMM}}$ and $n_{y-\mathrm{SMM}}$ are given by

$$n_{x-\mathrm{SMM}}^2 = \varepsilon_{x-\mathrm{SMM}}\mu_{x-\mathrm{SMM}} \tag{4}$$

$$n_{y-\mathrm{SMM}}^2 = \varepsilon_{y-\mathrm{SMM}}\mu_{y-\mathrm{SMM}} \tag{5}$$

where $\mu_{x-\mathrm{SMM}}, \mu_{y-\mathrm{SMM}}$ are the effective permeabilities of the SMM, and $\mu_{x-\mathrm{SMM}} = \mu_{y-\mathrm{SMM}} = 1$. It is worthy to note that, the permittivity (ε_d) of doped GaAs can be estimated with a Drude model [29]–[31]

$$\varepsilon_d = \varepsilon_\infty \left(1 - \frac{\omega_p^2}{\omega^2 + i\omega\gamma}\right) \tag{6}$$

where ε_∞ is the high frequency dielectric constant, and ω is the angular frequency. Here, the plasma frequency ω_p and relaxation frequency γ are given by

$$\omega_p = \sqrt{\frac{Nq^2}{\varepsilon_0\varepsilon_\infty m^*}} \tag{7}$$

$$\gamma = \frac{q}{vm^*} \tag{8}$$

where q is the electron charge, N is the electron density (which is the same as doping level n_d), m^* is the electron effective mass, and ν is the electron mobility. Moreover, the electron effective mass m^* and electron mobility ν also vary with the carrier density N [23], [32].

From (2) to (8), we can conclude that $\varepsilon_{x-\mathrm{SMM}}$ and $\varepsilon_{y-\mathrm{SMM}}$ are mainly determined by the filling fraction f and the free-carrier density n_d of the doped GaAs, and the real parts of $\varepsilon_{x-\mathrm{SMM}}$ and $\varepsilon_{y-\mathrm{SMM}}$ at the wavelengths of 5 μm $\sim$ 50 μm are depicted in Fig. 3.

From Fig. 3, the SMM experiences strong EM resonance for x-polarized waves, whereas it shows almost no resonance for y-polarized waves. In addition, increasing the free carrier-density n_d or decreasing the filling fraction f will shift the resonance wavelength λ_0 to a shorter one, as shown in Fig. 3(a) and (c). In fact, the resonance wavelength λ_0 of the SMM can be designed anywhere above 15 μm by properly adjusting the free-carrier density n_d or the filling

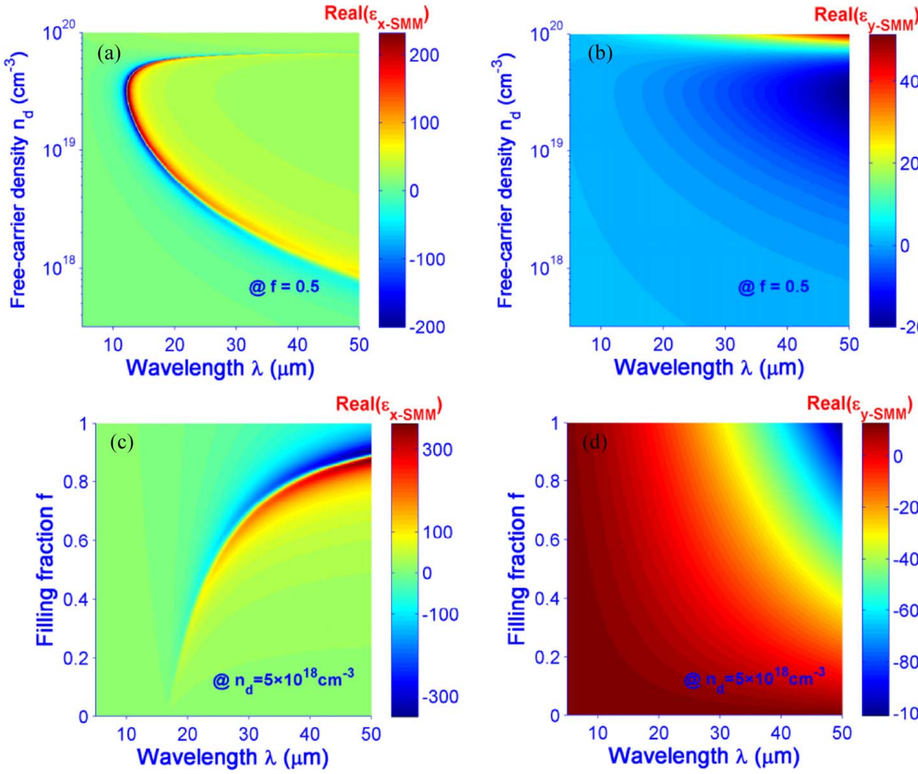

Fig. 3. (a) and (b) Real parts of $\varepsilon_{x-\mathrm{SMM}}$ and $\varepsilon_{y-\mathrm{SMM}}$ vary with free-carrier density n_d and wavelength for $f = 0.5$. (c) and (d) Real parts of $\varepsilon_{x-\mathrm{SMM}}$ and $\varepsilon_{y-\mathrm{SMM}}$ vary with f and wavelength for $n_d = 5 \times 10^{18}$ cm^{-3}.

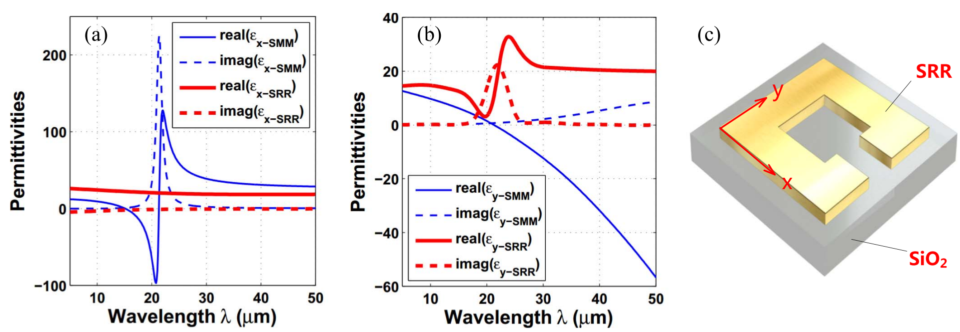

Fig. 4. Permittivities of the SMM and the SRRs along (a) the x direction and (b) the y direction. (c) Schematic of the SRR metamaterial unit.

fraction f. In the present work, we set $f = 0.5$, $n_d = 5 \times 10^{18}$ cm^{-3}, and plot the $\varepsilon_{x-\mathrm{SMM}}$ and $\varepsilon_{y-\mathrm{SMM}}$ of the SMM with blue lines in Fig. 4(a) and (b), respectively. The results show that the resonance wavelength of SMM is around 22 μm.

Since the SMM experiences strong EM resonance for x-polarized waves, then, in order to produce a large phase delay in the dual-metamaterial, the gold SRRs should exhibit EM resonance around 22 μm for y-polarized waves. Therefore, we construct a SRR metamaterial composed of gold SRRs and SiO_2 substrate (see Fig. 4(c)), and design the split of SRR to be parallel to the y-axis to excite electric responses to y-polarized waves, as shown in Fig. 1(b). We simulate its reflection-transmission data with COMSOL Multiphysics software, and extract the effective permittivities ($\varepsilon_{x-\mathrm{SRR}}$ and $\varepsilon_{y-\mathrm{SRR}}$) of the SRR metamaterial with these data via a

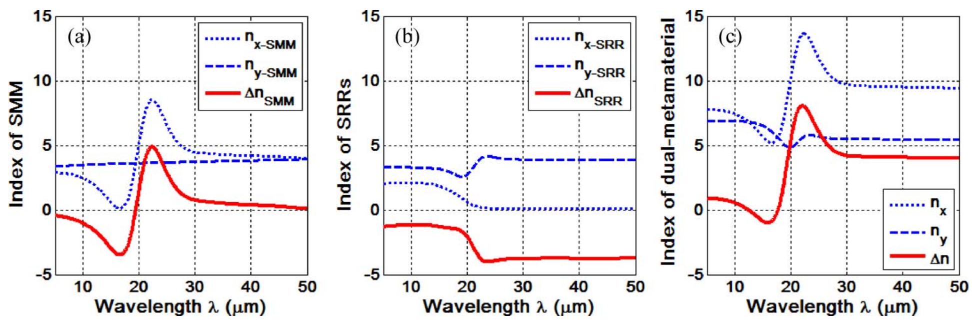

Fig. 5. Real parts of refractive indices and birefringence of (a) the SMM, (b) the SRRs, and (c) the dual-metamaterial.

retrieval procedure method [33], as shown with red lines in Fig. 4(a) and (b), respectively. The Finite Element Method with COMSOL Multiphysics are used in our numerical calculations. The simulated unit cell consists of Au SRR and SiO_2, as shown in Fig. 4(c). A plane wave with electric field polarized in the y direction normally impinges on the $x-y$ plane. In the simulation, the incident plane wave comes from the user defined "port excitation" in the RF module of the COMSOL software; in addition, to account for the periodic nature of the metamaterial, the model boundaries normal to x direction and y direction are set to be periodic boundary condition. The geometrical sizes of the Au SRR and substrate SiO_2 are given in Section 2, and the permittivity of bulky gold can be described with Drude model, $\varepsilon_{\mathrm{Au}} = 1 - \omega_{p-\mathrm{Au}}^2/(\omega(\omega + i\omega_{c-\mathrm{Au}}))$, where $\omega_{p-\mathrm{Au}} = 2\pi \times 2.175 \times 10^{15}\ s^{-1}$ and $\omega_{c-\mathrm{Au}} = 2 \times 6.5 \times 10^{12}\ s^{-1}$ are the plasma frequency and collision frequency, respectively [34]–[36].

As is expected, both the resonance wavelengths of the SMM and the SRRs are close to the desired value of 22 μm, as shown in Fig. 4(a) and (b). To better understand the resonance mechanism of the dual-metamaterials, we calculate the real parts of refractive indices and birefringence for the SMM, the SRRs and the dual-metamaterials in Fig. 5(a)–(c), respectively. In these calculations, the real parts of refractive indices and birefringence for the SMM, i.e., $n_{x-\mathrm{SMM}}$, $n_{y-\mathrm{SMM}}$ and $\Delta n_{\mathrm{SMM}} = n_{x-\mathrm{SMM}} - n_{y-\mathrm{SMM}}$, are calculated by using (4) and (5); those for the SRRs, i.e., $n_{x-\mathrm{SRR}}$, $n_{y-\mathrm{SRR}}$ and $\Delta n_{\mathrm{SRR}} = n_{x-\mathrm{SRR}} - n_{y-\mathrm{SRR}}$, are obtained by employing the abovementioned retrieval procedure [33], and those for the dual-metamaterial are calculated by $n_x = n_{x-\mathrm{SMM}} - n_{x-\mathrm{SRR}}$, $n_y = n_{y-\mathrm{SMM}} - n_{y-\mathrm{SRR}}$, and $\Delta n = n_x - n_y$.

It can be seen from Fig. 5 that the dual-metamaterial will have more remarkable birefringence than the SMM and the SRRs. For instance, around the wavelength of 22 μm, the maximal birefringence Δn_{SMM} of the SMM is less than 5 (see Fig. 5(a)), and that of the SRRs is less than 4 (see Fig. 5(b)), whereas for the dual-metamaterial, the maximal birefringence Δn reaches 7.5 (see Fig. 5(c)).

To more clearly and directly show their birefringence, we also simulate the transmission phases of the SMM and SRRs, as shown in Fig. 6. In these simulations, $\Delta\varphi_{x-\mathrm{SMM}}$ and $\Delta\varphi_{y-\mathrm{SMM}}$ denote the phase shifts of SMM for x-polarized wave and y-polarized wave, respectively; $\Delta\varphi_{x-\mathrm{SRR}}$ and $\Delta\varphi_{y-\mathrm{SRR}}$ denote the phase shifts of SRRs for x-polarized wave and y-polarized wave, respectively; and $\Delta\varphi_{\mathrm{SMM}} = \Delta\varphi_{x-\mathrm{SMM}} - \Delta\varphi_{y-\mathrm{SMM}}$ and $\Delta\varphi_{\mathrm{SRR}} = \Delta\varphi_{y-\mathrm{SRR}} - \Delta\varphi_{x-\mathrm{SRR}}$ are the phase delays between the two orthogonally polarized components for the SMM and SRRs, respectively.

As we can see from Fig. 6, due to the birefringence, both the SMM and SRRs appear obvious phase delay around resonance wavelengths. To further illustrate the larger birefringence of the dual-metamaterial, we also simulate the transmissions (t_x and t_y) and phases (φ_x and φ_y) of the transmission EM waves for the dual-metamaterial, and depict them in Fig. 7(a) and (b). Here, $t_x = |E_{xt}/E_{xi}|$ and $t_y = |E_{yt}/E_{yi}|$, where E_{xt} and E_{yt} represent the electric field of the x-polarized and y-polarized transmission waves, respectively; and E_{xi} and E_{yi} are those for the incident waves. Here, the simulated unit cell of the dual metamaterial consists of Au SRR, SiO_2, and SMM, as shown in Fig. 1(b); the geometrical sizes of the Au SRR, substrate SiO_2, and SMM are

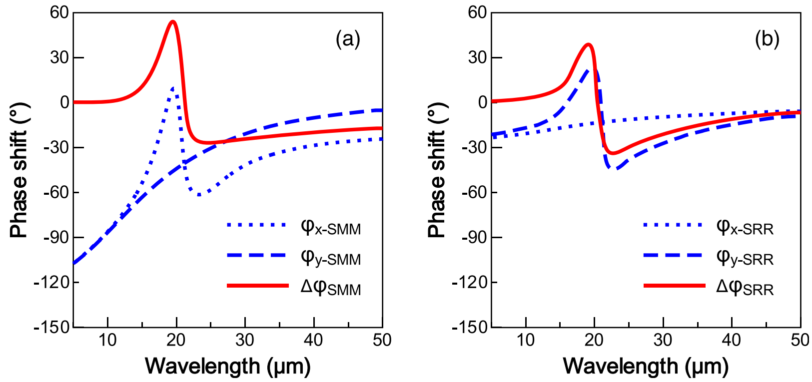

Fig. 6. Transmission phases of (a) the SMM and (b) SRRs.

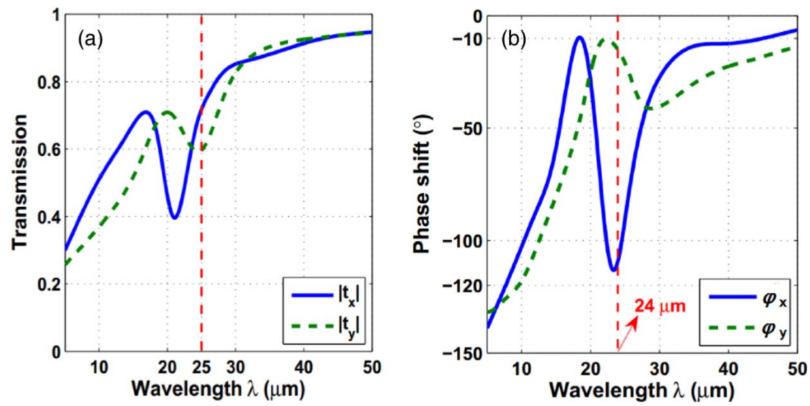

Fig. 7. (a) Transmissions $|t_x|$ and $|t_y|$ and (b) phase shifts φ_x and φ_y of the dual-metamaterial for the x-polarized and y-polarized components.

given in Section 2; and the calculated permittivities ($\varepsilon_{x-\mathrm{SMM}}$ and $\varepsilon_{y-\mathrm{SMM}}$) of SMM are also used in these simulations. As is expected, the dual-metamaterial indeed have resonance effects in both x-polarized direction and y-polarized direction. Additionally, due to that the SMM exhibits stronger EM resonance than the SRRs, as described in Fig. 5, the dual-metamaterial exhibits stronger resonance effect for x-polarized waves than for the y-polarized waves. More importantly, the dual-metamaterial has large birefringence due to the resonance, for example, at the wavelength of 24 μm, phase difference $\Delta\varphi$ ($\Delta\varphi = |\varphi_x - \varphi_y|$) is about 90°, as shown in Fig. 7(b), and this can not be accomplished by single-layer metamaterials, as mentioned in Section 1. Meanwhile, transmission $|t_x|$ is almost equal to $|t_y|$ at 24 μm, as shown in Fig. 7(a). This implies that this dual-metamaterial can work as a very compact quarter-wave plate around 24 μm wavelength. The thickness of its operation medium, $t_1 + t_2 + t_3$, is only 0.58 μm. Therefore, the quarter-wave plate based on dual-metamaterial is much thinner than conventional quarter-wave plates made of crystals or polymers, and it is also thinner than other metamaterial-based wave plates.

We are also reminded that the resonance wavelength of the dual-metamaterial for y-polarized EM waves no longer locates at 22 μm but shifts to 25 μm, as indicated by the red-dash line in Fig. 7(a). Noting that the resonance effect for y-polarized waves are contributed by the SRRs, as stated above, we can find the reason for the shift in resonance wavelength. When we calculate the resonance wavelength (22 μm) of the SRR metamaterial (the corresponding results are shown in Fig. 4(b)), the substrate of the gold SRRs is the SiO_2 layer (see Fig. 4(c)); and when we calculate the resonance wavelength of the dual-metamaterial, the effective substrate of the gold SRRs are the SiO_2 layer and the SMM layer. As we know, the thickness and refractive index of the substrate influence the resonance wavelength of a metamaterial [37], [38], for example, increasing the thickness or the refractive index of a substrate will lead to a red shift in resonance peak. In present work, the effective refractive index of the SMM is over 3.8, as shown in Fig. 5(a), which is obviously larger than that of SiO_2 [39], [40]; therefore, the effective refractive index of the SiO_2 layer and SMM layer will be larger than that of SiO_2 layer. Moreover, the thickness of the effective substrate (SiO_2 layer and SMM layer) is also larger than before (SiO_2 layer). As a result, the resonance wavelength of the dual-metamaterial for *y*-polarized EM waves shifts to a longer one.

4. Conclusion

In summary, in order to enhance birefringence of wave plates, we introduce a dual-metamaterial composed of a SMM and SRRs. Due to that the SMM and the SRRs respond to different polarization components of the EM wave, the dual-metamaterial has a higher refractive index difference between the two orthogonal polarization components. Within only 0.58 μm-thick operation medium, the dual-metamaterial is capable of producing a considerable phase delay (~90°) and serving as a very compact quarter-wave plate. Although the operation wavelength is within mid-infrared regime in this work, it can be extended to other spectral regions, such as terahertz and microwave bands, by adjusting the structure parameters of the SRRs and SMM. We believe that the concept of dual-metamaterial may enable us to implement other high-performance, ultra-compact micro/nano-optical devices and components.

References

[1] D. Kaufman, A. Sa'ar, and N. Kuze, "Anisotropy, birefringence, and optical phase retardation related to intersubband transitions in multiple quantum well structures," *Appl. Phys. Lett.*, vol. 64, no. 19, pp. 2543–2545, 1994.
[2] L. Bouchenoire, R. J. Morris, and T. P. Hase, "A silicon <111> phase retarder for producing circularly polarized X-rays in the 2.1-3 keV energy range," *Appl. Phys. Lett.*, vol. 101, no. 6, 2012, Art. ID 064107.
[3] H. Ren, Y.-H. Lin, and S.-T. Wu, "Linear to axial or radial polarization conversion using a liquid crystal gel," *Appl. Phys. Lett.*, vol. 89, no. 5, 2006, Art. ID 051114.
[4] P. Wang and A. Asundi, "A whole-field polariscope using a liquid crystal polarization rotator," *Rev. Sci. Instrum.*, vol. 79, 2008, Art. ID 063105.
[5] Z. Marcet *et al.*, "A half wave retarder made of bilayer subwavelength metallic apertures," *Appl. Phys. Lett.*, vol. 98, no. 15, 2011, Art. ID 151107.
[6] X. G. Peralta *et al.*, "Metamaterials for THz polarimetric devices," *Opt. Express*, vol. 17, no. 2, pp. 773–783, 2009.
[7] P. Weis, O. Paul, C. Imhof, R. Beigang, and M. Rahm, "Strongly birefringent metamaterials as negative index terahertz wave plates," *Applied Physics Letters*, vol. 95, no. 17, 2009, Art. ID 171104.
[8] M. Iwanaga, "Ultracompact waveplates: Approach from metamaterials," *Appl. Phys. Lett.*, vol. 92, no. 15, 2008, Art. ID 53102.
[9] A. A. Zharov, N. A. Zharova, R. E. Noskov, I. V. Shadrivov, and Y. S. Kivshar, "Birefringent left-handed metamaterials and perfect lenses for vectorial fields," *New J. Phys.*, vol. 7, pp. 220-1–220-9, 2005.
[10] C. Imhof and R. Zengerle, "Strong birefringence in left-handed metallic metamaterials," *Opt. Commun.*, vol. 280, no. 1, pp. 213–216, Dec. 2007.
[11] Y. M. Strelniker and D. J. Bergman, "Strong angular magneto-induced anisotropy of Voigt effect in metal-dielectric metamaterials with periodic nanostructures," *Phys. Rev. B*, vol. 89, no. 12, 2014, Art. ID 125312.
[12] G. V. Naik and A. Boltasseva, "Semiconductors for plasmonics and metamaterials," *Physica Status Solidi (RRL)-Rapid Res. Lett.*, vol. 4, no. 10, pp. 295–297, Oct. 2010.
[13] H. Li *et al.*, "Polarization and transmission properties of metamaterial-based three-dimensional plasmonic structure," *IEEE Photon. J.*, vol. 3, no. 3, pp. 400–406, Jun. 2011.
[14] B. Wang, X. Zhai, G. Wang, W. Huang, and L. Wang, "Design of a four-band and polarization insensitive terahertz metamaterial absorber," *IEEE Photon. J.*, vol. 7, no. 1, Feb. 2015, Art. ID 4600108.
[15] N. Yogesh, T. Fu, F. Lan, and Z. Ouyang, "Far-infrared circular polarization and polarization filtering based on Fermat's spiral chiral metamaterial," *IEEE Photon. J.*, vol. 7, no. 3, Jun. 2015, Art ID. 4600212.
[16] Z. Yang and S. Ramanathan, "Breakthroughs in Photonics 2014: Phase change materials for Photonics," *IEEE Photon. J.*, vol. 7, no. 3, Jun. 2015, Art. ID 0700305.
[17] W. Withayachumnankul and D. Abbott, "Metamaterials in the terahertz regime," *IEEE Photon. J.*, vol. 1, no. 2, pp. 99–118, Aug. 2009.
[18] J.-B. Masson and G. Gallot, "Terahertz achromatic quarter-wave plate," *Opt. Lett.*, vol. 31, no. 2, pp. 265–267, 2006.
[19] B. Scherger, M. Scheller, N. Vieweg, S. T. Cundiff, and M. Koch, "Paper terahertz wave plates," *Opt. Exp.*, vol. 19, no. 25, pp. 24884–24889, 2011.
[20] P. Hariharan, "Achromatic and apochromatic halfwave and quarterwave retarders," *Opt. Eng.*, vol. 35, no. 11, pp. 3335–3337, 1996.

[21] B. Boulbry, B. Bousquet, B. Le Jeune, Y. Guern, and J. Lotrian, “Polarization errors associated with zero-order achromatic quarter-wave plates in the whole visible spectral range,” *Opt. Express*, vol. 9, no. 5, pp. 225–235, 2001.
[22] M. Scheller, C. Jördens, and M. Koch, “Terahertz form birefringence,” *Opt. Exp.*, vol. 18, no. 10, pp. 10137–10142, 2010.
[23] A. J. Hoffman *et al.*, “Negative refraction in semiconductor metamaterials,” *Nature Mater.*, vol. 6, pp. 946–950, 2007.
[24] R. Maas, J. Parsons, N. Engheta, and A. Polman, “Experimental realization of an epsilon-near-zero metamaterial at visible wavelengths,” *Nature Photon.*, vol. 7, pp. 907–912, 2013.
[25] T. Xu, A. Agrawal, M. Abashin, K. J. Chau, and H. J. Lezec, “All-angle negative refraction and active flat lensing of ultraviolet light,” *Nature*, vol. 497, pp. 470–474, 2013.
[26] X. Hu, Y. Zhang, Y. Fu, H. Yang, and Q. Gong, “Low-power and ultrafast all-optical tunable nanometer-scale photonic metamaterials,” *Adv. Mater.*, vol. 23, no. 37, pp. 4295–4300, Oct. 2011.
[27] J. Valentine *et al.*, “Three-dimensional optical metamaterial with a negative refractive index,” *Nature*, vol. 455, pp. 376–379, 2008.
[28] A. Husakou and J. Herrmann, “Steplike transmission of light through a metal-dielectric multilayer structure due to an intensity-dependent sign of the effective dielectric constant,” *Phys. Rev. Lett.*, vol. 99, no. 12, Sep. 2007, Art. ID 127402.
[29] Y. C. Jun *et al.*, “Active tuning of mid-infrared metamaterials by electrical control of carrier densities,” *Opt. Exp.*, vol. 20, no. 2, pp. 1903–1911, 2012.
[30] X. Miao *et al.*, “Doping tunable resonance: Toward electrically tunable mid-infrared metamaterials,” *Appl. Phys. Lett.*, vol. 96, 2010, Art. ID 101111.
[31] C. Kittel, *Introduction to Solid State Physics*. Hoboken, NJ, USA: Wiley, 2005.
[32] P. Huggard *et al.*, “Drude conductivity of highly doped GaAs at terahertz frequencies,” *J. Appl. Phys.*, vol. 87, no. 5, pp. 2382–2385, 2000.
[33] D. Smith, D. Vier, T. Koschny, and C. Soukoulis, “Electromagnetic parameter retrieval from inhomogeneous metamaterials,” *Phys. Rev. E*, vol. 71, no. 3, Mar. 2005, Art. ID 036617.
[34] P. B. Johnson and R.-W. Christy, “Optical constants of the noble metals,” *Phys. Rev. B*, vol. 6, no. 12, pp. 4370–4379, Dec. 1972.
[35] M. A. Ordal, R. J. Bell, R. Alexander, Jr, L. Long, and M. Querry, “Optical properties of fourteen metals in the infrared and far infrared: Al, Co, Cu, Au, Fe, Pb, Mo, Ni, Pd, Pt, Ag, Ti, V, and W,” *Appl. Opt.*, vol. 24, no. 24, pp. 4493–4499, 1985.
[36] S. Linden *et al.*, “Magnetic response of metamaterials at 100 terahertz,” *Science*, vol. 306, no. 5700, pp. 1351–1353, 2004.
[37] D. Park, S. Park, I. Park, and Y. Ahn, “Dielectric substrate effect on the metamaterial resonances in terahertz frequency range,” *Current Appl. Phys.*, vol. 14, pp. 570–574, Apr. 2014.
[38] Z. Sheng and V. V. Varadan, “Tuning the effective properties of metamaterials by changing the substrate properties,” *J. Appl. Phys.*, vol. 101, no. 1, 2007, Art. ID 014909.
[39] C. Kittel and P. McEuen, *Introduction to Solid State Physics*, vol. 8. New York, NY, USA: Wiley, 1976.
[40] M. Wakaki, T. Shibuya, and K. Kudo, *Physical Properties and Data of Optical Materials*. Boca Raton, FL: CRC, 2010.